IOPscience iopscience.iop.org

Home Search Collections Journals About Contact us My IOPscience

Above-threshold ionization of atoms by resonant XUV laser pulses

This article has been downloaded from IOPscience. Please scroll down to see the full text article.

2011 J. Phys. B: At. Mol. Opt. Phys. 44 125603

(http://iopscience.iop.org/0953-4075/44/12/125603)

View the table of contents for this issue, or go to the journal homepage for more

Download details:
IP Address: 157.92.4.12
The article was downloaded on 26/04/2012 at 14:48

Please note that terms and conditions apply.

J. Phys. B: At. Mol. Opt. Phys. **44** (2011) 125603 (8pp) doi:10.1088/0953-4075/44/12/125603

Above-threshold ionization of atoms by resonant XUV laser pulses

V D Rodríguez[1], D G Arbó[2] and P A Macri[3]

[1] Departamento de Física and IFIBA-CONICET, FCEyN, Universidad de Buenos Aires, 1428 Buenos Aires, Argentina
[2] Instituto de Astronomía y Física del Espacio, FCEN-UBA CONICET, CC 67 Suc 28 Buenos Aires, Argentina
[3] Departamento de Física, FCEyN, Instituto de Investigaciones Físicas de Mar del Plata (IFIMAR), Universidad Nacional de Mar del Plata-CONICET, Funes 3350, 7600 Mar del Plata, Argentina

E-mail: vladimir@df.uba.ar

Received 28 January 2011, in final form 6 May 2011
Published 8 June 2011
Online at stacks.iop.org/JPhysB/44/125603

Abstract
Above-threshold ionization of atoms by XUV short laser pulses with frequencies close to the resonant 1s–2p transition is investigated. We present a theory based on a variational expression using trial wavefunctions for the final and the initial states. For the former we use a Coulomb–Volkov wavefunction, and for the latter a close-coupling solution of the time-dependent Schrödinger equation considering a few bound states. The close-coupling Coulomb–Volkov theory, fully accounting for the important 1s–2p transition, explains the photoelectron spectrum as well as the total ionization cross sections for the resonant case. We also compare the partial wave populations and angular distributions given by the theory with the numerical solutions of the time-dependent Schrödinger equation.

(Some figures in this article are in colour only in the electronic version)

1. Introduction

Three decades ago, the observation of photoelectron energy spectra containing series of equispaced peaks exceeding the photon minimum number needed to reach the ionization threshold, known today as above-threshold ionization (ATI), was the first experimental manifestation of non-perturbative strong-field light–matter interactions [1]. The atomic or molecular electron ionization by a short and intense laser pulse takes place through sequential absorption of several photons. At each step, the electron acquires a higher energy usually lying far from any field-dressed state energy. Consequently, the electron spends only a short time there (of the order of an optical cycle) before eventually decaying to lower energy levels unless it absorbs another photon. If, on the contrary, the photon frequency is tuned close to an intermediate field-dressed state resonance, the electron will remain in that state much longer, enhancing the probability of the multiphoton process [2, 3].

Nowadays, resonance enhanced ATI has been observed in different contexts. Experiments with rare gases exhibit a rescattering plateau enhancement for sharply defined laser intensities [4–6]. In several theoretical works [7–9], the enhancements are explained by multiphoton resonance with the ponderomotively upshifted threshold. These types of resonances, known as Freeman resonances [10], are usually regarded as multiphoton ionization indicators. They are evident in photoelectron spectra when multiphoton excitation leads to a population of Rydberg states ionized afterwards. A note of caution should be made on the interpretation of the origin of the enhancements since this phenomena have been explained by other authors as a channel-closing effect [6, 11].

Resonance signatures with a bouquet-like pattern have been recently observed in noble-gases ATI parallel-transverse low-momentum distributions [12]. Surprisingly, the measured longitudinal momentum distributions with ATI-like structures survive deep in the tunnelling regime. The atomic structure plays a minor role in the formation of the low-energy photoelectron spectra even in the high-intensity regime, as proved in [13]. The observed spectral structures in the longitudinal momentum distributions have been interpreted using a resonant ionization model [14]. The measurements have been understood as resonant-enhanced ionization through Rydberg states [10]. Moreover, the inspection of the

 © 2011 IOP Publishing Ltd Printed in the UK & the USA

electron kinetic energy spectra and the angular distributions of the resonantly ionized electrons allowed the intermediate Rydberg states involved in the ionization process to be reliably identified. These results are in agreement with theoretical analysis in [15] where experiments were interpreted by means of direct and resonant ionization models. Thus, identification of specific resonant Rydberg states at particular intensities has been achieved.

The ATI photoelectron spectrum also shows resonance effects due to deeper bound field-dressed states. In [16], the photoelectron spectra of positronium irradiated by short laser pulses present doublets in relation to the bound–bound resonance known as Autler–Townes doublets [17]. The ATI peak splitting, a consequence of Rabi oscillations, was described by means of a two-state Coulomb–Volkov approximation [16]. Previous non-perturbative semi-analytical theories [18, 19] have considered the time-dependent final continuum wavefunction as a Coulomb–Volkov approximation and the initial state as a field-unperturbed bound state. This simple description of the initial state is not reliable for processes where an intermediate field-dressed state is populated by a resonant tuned laser frequency. For this reason, the initial state description was improved by an exact two-state close-coupling calculation, when the positronium 1s–2p$_0$ transition was investigated in [16]. The same process was studied in [20] for hydrogen atoms. Their results for the exact solution of the time-dependent Schrödinger equation (TDSE) were interpreted by a simple model considering Rabi flopping dynamics as the zeroth-order solution to the problem of infinite number of bound states coupled to the continuum by a laser field. However, the rotating wave approximation was considered.

In this paper, a further improvement of [16] is performed using an n-state exact close-coupling initial state and applying it to investigate enhancements in the total ionization probability. The appearance of new structures in the ATI photoelectron spectra of hydrogen atoms due to the influence of intermediate states is analysed.

The paper is organized as follows. In section 2, we introduce our theoretical formulation. Results showing the main qualitative features of the photoelectron spectra and the total ionization probability are presented in section 3. Section 4 contains our main conclusions and perspectives. Atomic units are used throughout unless otherwise stated.

2. Theory

We consider here the ionization of a one-active electron atom by an external laser radiation with the electric field $\mathbf{F}(t)$ given by

$$\mathbf{F}(t) = \mathbf{F}_0 \sin(\omega t + \varphi) \sin^2\left(\frac{\pi t}{\tau}\right), \tag{1}$$

between $t = 0$ and τ, and zero otherwise. In equation (1), τ is the pulse duration, ω is the laser carrier frequency and $\mathbf{F_0}$ determines the field amplitude and polarization direction. Under non-relativistic conditions and within the electric dipole approximation the electron wavefunction $\Psi(\mathbf{r}, t)$ satisfies the TDSE which, written in the length gauge, reads

$$\mathrm{i}\frac{\mathrm{d}\Psi(\mathbf{r}, t)}{\mathrm{d}t} = \left[-\frac{1}{2}\nabla^2 + V(r) + \mathbf{r}\cdot\mathbf{F}(\mathbf{t})\right]\Psi(\mathbf{r}, t), \tag{2}$$

where $\mathbf{r}$ is the position of the electron with respect to the much heavier positive ion and $V(r)$ is the interaction between the electron and the rest of the target.

The transition amplitude from the state i at $t = 0$ to the state f at $t = \tau$ may be approximated by the prior and post forms of the following variational expression [21]:

$$a_{fi}^{-} = \lim_{t\to 0}\langle\chi_f^{-}(t)|\chi_i^{+}(t)\rangle - \mathrm{i}\int_0^\tau \mathrm{d}t\langle\chi_f^{-}(t)|\overleftarrow{H - \mathrm{i}\frac{\mathrm{d}}{\mathrm{d}t}}|\chi_i^{+}(t)\rangle \tag{3}$$

$$a_{fi}^{+} = \lim_{t\to \tau}\langle\chi_f^{-}(t)|\chi_i^{+}(t)\rangle - \mathrm{i}\int_0^\tau \mathrm{d}t\langle\chi_f^{-}(t)|\overrightarrow{H - \mathrm{i}\frac{\mathrm{d}}{\mathrm{d}t}}|\chi_i^{+}(t)\rangle, \tag{4}$$

respectively, where the arrows on the right-hand side indicate the state on which the non-Hermitian operator applies; $\chi_f^{-}(t)$ and $\chi_i^{+}(t)$ are trial functions to the exact solutions to equation (2), subject to the initial and final state conditions:

$$\lim_{t\to\tau}\chi_f^{-}(t) = \phi_f^{-}(\mathbf{r}, t) = \varphi_f^{-}(\mathbf{r})\exp(-\mathrm{i}\epsilon_f t), \tag{5}$$

$$\lim_{t\to 0}\chi_i^{+}(t) = \phi_i^{+}(\mathbf{r}, t) = \varphi_i^{+}(\mathbf{r})\exp(-\mathrm{i}\epsilon_i t). \tag{6}$$

In (5) and (6), $\varphi_f^{-}(\mathbf{r})$ and $\varphi_i^{+}(\mathbf{r})$ are eigenfunctions of the atomic Hamiltonian associated with the eigenenergies ϵ_f and ϵ_i, respectively. Equations (3) and (4) provide exact transition amplitudes when one of the two trial functions are exact solutions of equation (2). In [18, 19], the Coulomb–Volkov wavefunction was used as the trial final wavefunction

$$\chi_f^{-}(\mathbf{r}, t) = \phi_f^{-}(\mathbf{r}, t)\exp\left[\mathrm{i}\mathbf{A}^{-}(t)\cdot\mathbf{r} - \mathrm{i}\,\mathbf{k}\cdot\int_\tau^t \mathrm{d}t'\mathbf{A}^{-}(t') - \frac{\mathrm{i}}{2}\int_\tau^t \mathrm{d}t'\mathbf{A}^{-2}(t')\right], \tag{7}$$

where $\mathbf{A}^{-}(t) = \int_t^\tau \mathrm{d}t'\ \mathbf{F}(t')$ is the vector potential and $\mathbf{k}$ is the electron momentum. Introducing the Coulomb–Volkov wavefunction of equation (7) in the transition amplitude (3), we can easily obtain the expression

$$a_{fi}^{-} = \int_0^\tau \mathrm{d}t\exp\left\{\mathrm{i}\frac{k^2}{2}t + \mathrm{i}\mathbf{k}\cdot\int_\tau^t \mathrm{d}t'\mathbf{A}^{-}(t') + \frac{\mathrm{i}}{2}\int_\tau^t \mathrm{d}t'\mathbf{A}^{-2}(t')\right\} \times \int \mathrm{d}\mathbf{r}\ \chi_i^{+}(\mathbf{r}, t)\exp[\mathrm{i}\mathbf{A}^{-}(t)\cdot\mathbf{r}]\mathbf{A}^{-}(t)\cdot[\mathrm{i}\mathbf{k} + \nabla]\varphi_f^{-*}(r). \tag{8}$$

The choice of the appropriate trial wavefunction $\chi_i^{+}(\mathbf{r}, t)$ in equation (8) will depend on the process to be described. For photon energies above the ionization threshold and for intensities small enough to ensure a total ionization probability far from the saturation regime, the unperturbed initial wavefunction $\varphi_i^{+}(\mathbf{r})\exp(-\mathrm{i}\epsilon_i t)$ can be safely used. This has been performed in the framework of the Coulomb–Volkov (CV2$^-$) theory where a favourable comparison with exact TDSE computations has been found within the aforementioned

conditions [18, 19]. However, for photon energies below the ionization threshold a better description of the initial trial wavefunction is required. In this case, the electron will absorb several photons during the ionization process, passing through many virtual intermediate states. Even when the photon energy is not in tune, the wide spectrum of the short laser pulse allows population of the excited states. This effect is observed in the appearance of secondary peaks on the ATI photoelectron spectrum and can be interpreted as different multiphoton ionization channels launched from every relevant field-dressed excited state. A simple way to improve the CV2$^-$ taking these channels into account is to consider a different choice for the trial wavefunction [22]

$$\chi_i^+(\mathbf{r},t) = \sum_j b_{ji}(t)\phi_j(\mathbf{r},t), \tag{9}$$

where $b_{ji}(t)$ is the transition amplitude at time t from the initial state ϕ_i to the intermediate state ϕ_j. In [22], $b_{ji}(t)$ was estimated by the first Born approximation giving place to the so-called modified Coulomb–Volkov (MCV2$^-$) approximation. Although MCV2$^-$ allows us to describe the position of the emergent secondary peaks, some sizable quantitative differences with TDSE remain. In this work, we improve MCV2$^-$ further, computing $b_{ji}(t)$ by solving the TDSE for $\chi_i^+(\mathbf{r},t)$ in an exact $N+1$-state (the initial plus N excited states) close-coupling scheme:

$$\dot{\mathbf{b}} = -\mathrm{i}(\mathbf{H}_0 + \mathbf{V})\mathbf{b}, \tag{10}$$

where $\mathbf{b}^\dagger = (b_{1i}, b_{2i}, \ldots, b_{N+1i})$, $\mathbf{H}_0$ is a diagonal matrix with the corresponding $N+1$ unperturbed energies, and $\mathbf{V}_{jj'} = \langle\phi_j|\mathbf{F}(t)\cdot\mathbf{r}|\phi_{j'}\rangle$ is the perturbation potential matrix. This first-order ordinary differential equation system has been solved using the splitting operator iterative procedure

$$\mathbf{b}(t+\Delta t) = \exp(-\mathrm{i}\mathbf{H}_0\Delta t/2)\exp(-\mathrm{i}\mathbf{V}\Delta t) \times \exp(-\mathrm{i}\mathbf{H}_0\Delta t/2)\mathbf{b}(t). \tag{11}$$

The exponential of the diagonal $\mathbf{H}_0$ is trivial. The exponential of the non-diagonal $\mathbf{V}$ is made by diagonalizing the $\mathbf{V}$. Note that for linear polarization this has to be done only once as the time-dependent part can be factorized.

Thus, the transition amplitude for the new close-coupling Coulomb–Volkov (CC-CV2$^-$) theory takes the form

$$a_{fi}^{\mathrm{CC-CV2-}} = \sum_{j=1}^{N+1}\int_0^\tau \mathrm{d}t\; b_{ji}(t)\exp\left\{\mathrm{i}k^2t/2 + \mathrm{i}\mathbf{k}\cdot\int_\tau^t \mathrm{d}t'\mathbf{A}^-(t') + \mathrm{i}/2\int_\tau^t \mathrm{d}t'\mathbf{A}^{-2}(t')\right\} \times \int \mathrm{d}\mathbf{r}\;\phi_j(\mathbf{r},t)\exp[\mathrm{i}\mathbf{A}^-(t)\cdot\mathbf{r}]\mathbf{A}^-(t)\cdot[\mathrm{i}\mathbf{k}+\nabla]\varphi_f^*(\mathbf{r}), \tag{12}$$

where j stands for the set of quantum numbers corresponding to the initial ($j=1$) and the first N excited states ($2 \leqslant j \leqslant N+1$). We observe that the first term in the sum goes to the standard CV2$^-$ when the simplest choice $b_{11}(t) = 1$ has been made. Other terms in the sum represent a series of CV2$^-$-like amplitudes for transitions starting from intermediate states j. These amplitudes are time integrals weighed by the close-coupling transition amplitudes at any time during the laser pulse. The interpretation of equation (12) is straightforward; every bound state is populated with an amplitude given by $b_{ji}(t)$, achieved in this case through a close-coupling scheme among N+1 bound states. From every considered state a multiphoton promotion to the continuum is considered here by using a CV2$^-$-like amplitude. In this work, we have checked that the convergence is achieved in equation (12) for principal quantum numbers $n \leqslant 5$. The magnetic quantum number is a constant of motion. Thus, in what follows all states are understood to have $m = 0$. We find that secondary peaks for higher intermediate states vanish in the background.

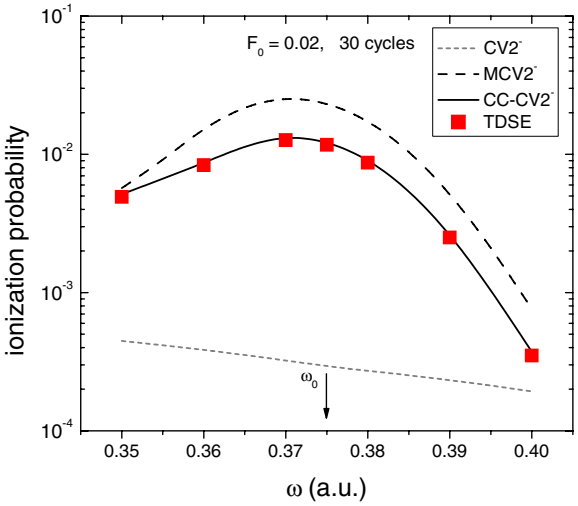

Figure 1. Total ionization probability as a function of the frequency ω of a laser pulse of 30-cycle duration and maximum amplitude $F_0 = 2\times10^{-2}$ au, corresponding to an intensity $I = 1.4\times10^{13}$ W cm^{-2}. Dotted line, CV2$^-$; dashed line, MCV2$^-$; solid line, CC-CV2$^-$; symbols, TDSE. The arrow indicates the resonance ω_0.

3. Results

In order to probe the CC-CV2$^-$ we focus on the ionization process of a hydrogen atom subject to a linearly polarized short-laser pulse, and compare the CC-CV2$^-$ results with previous and less elaborate CV2$^-$ and MCV2$^-$ [18, 19, 22]. As a final test of the CC-CV2$^-$, we also compare the above-mentioned approximations with the TDSE numerical solution [13]. Along this work, the laser frequencies considered are near the hydrogen 1s–2p resonance $\omega_0 = 0.375$ au.

We start by analysing the total ionization probability of a hydrogen atom initially in its ground state due to the laser field of equation (1) with a peak field $F_0 = 0.02$ au and total duration τ corresponding to 30 optical cycles. In figure 1, the total ionization probability as a function of the laser frequency may be seen. Whereas the CV2$^-$ results smoothly decrease with frequency, MCV2$^-$ results exhibit, as expected, an enhancement around ω_0 (indicated with an arrow) due to the ionization from the 2p state, included in the theory within the first Born approximation. Nevertheless, when compared with the TDSE results, the MCV2$^-$ overestimates the enhancement. On the other hand, the more complete CC-CV2$^-$, which improves the MCV2$^-$ by considering the populations of the bound states with a

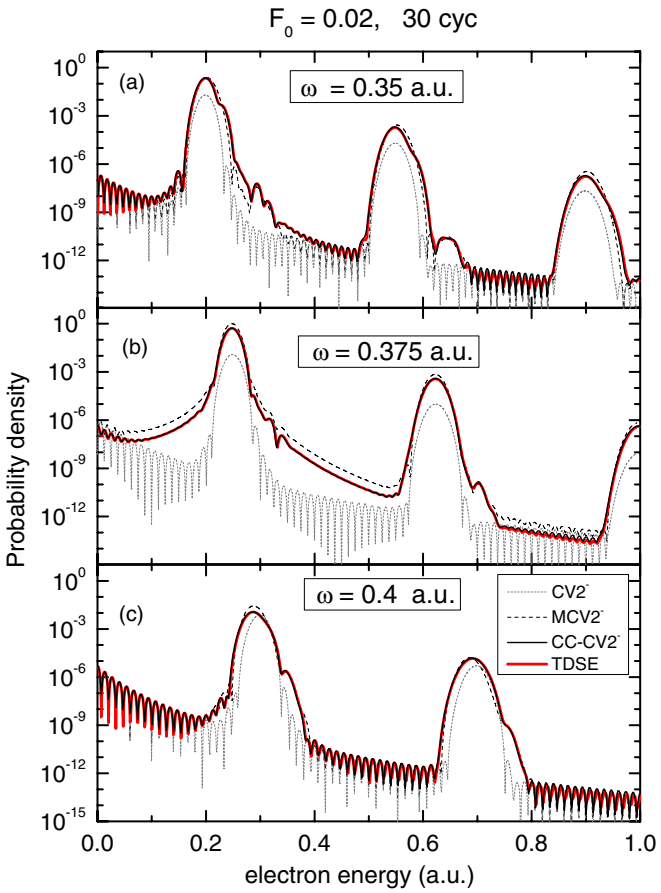

Figure 2. Energy distribution of ejected electrons as a function of the electron energy for three laser field frequencies: (a), $\omega = 0.35$ au; (b) $\omega = 0.375$ au; and (c) $\omega = 0.4$ au. Dotted line, CV2$^-$; dashed line, MCV2$^-$; solid line, CC-CV2$^-$; thick (red) solid line, TDSE. The maximum amplitude of the electric field is $F_0 = 2 \times 10^{-2}$ au corresponding to an intensity $I = 1.4 \times 10^{13}$ W cm^{-2}; the number of cycles is 30. CC-CV2$^-$ and TDSE curves are indistinguishable in this figure.

close-coupling approach, not only shows the enhancement around the resonance $\omega = \omega_0$, but also displays an excellent quantitative agreement with the TDSE computations.

In order to trace back the broad resonance in the total ionization probabilities, we examine the photoelectron spectrum. Figure 2 shows the electron energy distributions for three different frequencies: (a) below ($\omega = 0.35$), (b) at ($\omega = 0.375$) and (c) above ($\omega = 0.4$) the resonant case. In all cases, the CV2$^-$ provides multiphoton peaks well below those given by TDSE calculations. On the other hand, MCV2$^-$ appears to overestimate the ATI peaks, in particular, for the resonant case (b). The reason is that MCV2$^-$ has been calculated having $b_{11}(t) = 1$ in equation (12), which is not true as the initial ground state depopulates due to excitation and ionization. The condition $b_{11}(t) = 1$ also holds for CV2$^-$ which underestimates exact results. For a more realistic calculation, we used the CC-CV2$^-$ theory, which accounts accurately for all the ATI peaks when compared with TDSE in figure 2 for all frequencies considered.

In figure 2(a), a shoulder to the right of each main ATI peak and two resolved secondary peaks to the right of the first shoulder are observed. The shoulders arise from unresolved multiphoton ionization from the 2p level, and the secondary peaks come from multiphoton ionization from 3p and 4p states. This is corroborated by their locations at energies $\varepsilon_{Mn} = M\omega - 1/(2n^2)$, where M is the number of absorbed photons. In the case of the one-photon transition ($M = 1$) from 2p, 3p and 4p states, the secondary peaks are located at $E = 0.225$, 0.294 and 0.319, respectively. The two-photon process ($M = 2$) from the 2p, 3p and 4p states gives rise to one shoulder and two peaks at energies $E = 0.575$, 0.644 and 0.669, respectively. The MCV2$^-$ theory accounts for these pathways through intermediate states and, therefore, its results show the shoulders and the structure albeit with some numerical discrepancy. However, the present CC-CV2$^-$ theory, accounting for a more accurate population of the intermediate states, provides much better agreement when compared with the TDSE. The same pattern is valid for figure 2(c), but in this case the shoulders are actually to the left of the main ATI peaks, and the secondary peaks from 3p and 4p states are not well resolved. The corresponding positions are given for the one-photon transitions at 0.275 (2p), 0.344 (3p) and 0.369 (4p), and for the two-photon transitions at 0.675 (2p), 0.744 (3p) and 0.769 (4p).

The previous analysis allows us to understand the resonant case in figure 2(b). In this case, the location for the M-photon peak from the 2p state is the same as the $(M + 1)$-photon peak from the 1s state. But, the smaller the number of photons, the higher the probability and, therefore, a clear dominance of the population through the intermediate 2p state is expected. The CV2$^-$ theory is two orders of magnitude smaller than the TDSE results since it does not take into account the pathway through the resonant 2p-intermediate state (figure 2(b)). The positions of the first ($M = 1$) secondary peaks are resolved, and their values are 0.319 (3p) and 0.344 (4p). However, the second set ($M = 2$), located at 0.694 (3p) and 0.719 (4p), is not fully resolved. Again, CC-CV2$^-$ shows the best agreement when compared to the TDSE energy distributions, while the MCV2$^-$ shows the correct photoelectron structure, although it overestimates the TDSE results.

Now, we will analyse the background in the photoelectron spectra, i.e. the distribution for energies far from the mentioned ε_{Mn}. For both non-resonant cases (figures 2(a) and (c)), the simple CV2$^-$ roughly agrees with the more elaborate MCV2$^-$ and CC-CV2$^-$ theories, and with the TDSE computations in the background. However, differences among the theories arise at resonance even at the background level. TDSE computations in figure 2(b) display a considerable increase of the background in addition to the important enhancement of the ionization peaks. In this way, the simple CV2$^-$ drastically fails, underestimating the probability density by several orders of magnitude. Other features can be readily observed: the shape of the first peak within the MCV2$^-$ and the CC-CV2$^-$ around $E \simeq 0.25$ in figure 2(b) has a resemblance to the broad resonance observed in the first Born approximation for a single-photon transition to the continuum state. In turn, as stated before, the first CV2$^-$ peak is narrow, since it is formed by a two-photon process directly from the initial state and CV2$^-$ does not take into account the pathway through

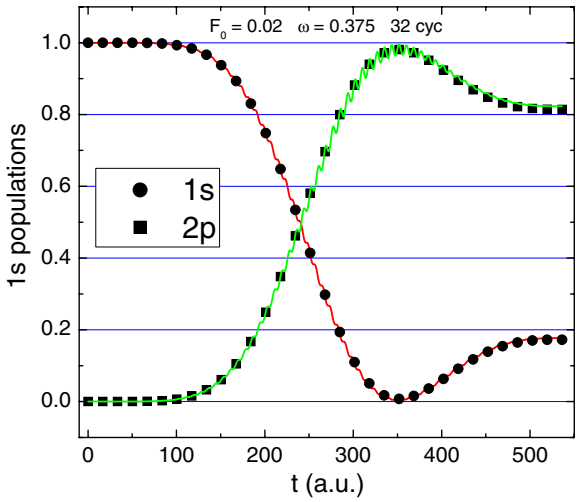

Figure 3. 1s and 2p populations for a 32-cycle laser pulse of maximum amplitude $F_0 = 2 \times 10^{-2}$ au at the resonance frequency $\omega = 0.375$ au. Solid line: CC-CV2$^-$, symbols: TDSE right after each of the cycles.

intermediate states. In addition, the case $\omega = 0.4$ au in figure 2(c) reveals that the first peak within the MCV2$^-$ (also CC-CV2$^-$ and TDSE) is broader and higher than the one corresponding to the CV2$^-$. This is due to the fact that it is not possible, in this case, to resolve between the first ATI peak ($E = 0.3$, coming from a two-photon transition from the 1s state) and the secondary peak ($E = 0.275$, coming from a single-photon transition from the 2p state). The contribution of the two ionization pathways leads to a shift of the multiphoton peaks to lower electron kinetic energies. However, some quantitative differences appear in MCV2$^-$ with respect to CC-CV2$^-$ and TDSE, since the former considers the transition amplitudes $b_{ij}(t)$ in equation (9) only within the first Born approximation.

So far, we find no detectable differences between TDSE and the more elaborate CC-CV2$^-$ energy distributions independent of the laser frequency. Only when the pathways through the transient intermediate states are accurately accounted for, in particular when the resonant 2p is properly included, can the theory describe the exact computations. This is particularly true when the field is weak and the pulse is short, so that no saturation of ionization probability exists. For the cases studied here, ionization probabilities are about or below 2% (see figure 1).

In order to prove that the correct inclusion of the 2p state is crucial to obtain right ionization yields, we compare the close coupling with TDSE populations of the 1s and 2p states as a function of time (figure 3). Both results resemble a typical Rabi oscillation which is partially washed out by the finite duration of the pulse. Close-coupling population looks like counter-rotating oscillations. TDSE populations were only computed when the electric field is zero and once per cycle. Figure 3 exhibits an excellent agreement between the close-coupling and TDSE probabilities. In recent works, the influence of Rabi oscillations on the splitting of ATI peaks has been considered in relation to the Autler–Townes effect, which has proven to be a splitting of the ATI peaks in the

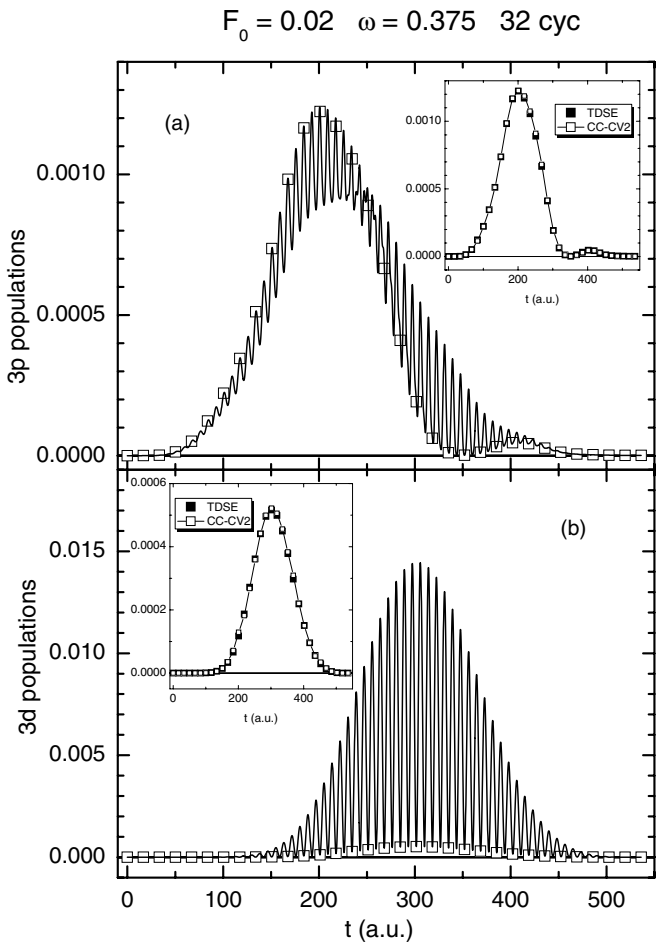

Figure 4. CC-CV2$^-$ (a) 3p and (b) 3d populations for a 32-cycle laser pulse of maximum amplitude $F_0 = 2 \times 10^{-2}$ au at the resonance frequency $\omega = 0.375$ au. The symbols indicate the value of the populations right after each of the 32 cycles. Inset: comparison of CC-CV2$^-$ (open symbols) and TDSE (full symbols) populations right after each cycle. Connecting lines in the insets are only for eye guidance.

photoelectron spectrum [16, 20]. Nevertheless, this non-perturbative effect is not present here since the pulse duration is shorter than one Rabi cycle. The only way to observe more Rabi cycles for a fixed pulse duration is by increasing the laser intensity, which would necessarily require a better treatment accounting for the depletion of the bound states.

We have also calculated other bound state populations different from the resonant 2p and initial ground states. In particular, time-dependent populations of the 3p state and the one corresponding to the 3d state calculated within the close-coupling approach are shown in figures 4(a) and (b), respectively. The oscillating pattern is more evident than in the populations of 1s and 2p states. The symbols show the values for discrete times when the electric field of equation (1) is zero and once per cycle, i.e. $t_i = i2\pi/\omega$, $i = 1, \ldots, N_{\rm cyc}$, (where $N_{\rm cyc}$ is the total number of cycles equal to $\tau\omega/2\pi$). Two main features may be observed. First, bound state populations, different from resonant 2p and initial 1s, are below 0.015 and, therefore, play practically no role in the ionization dynamics. Second, a minimum in the 3p population is observed close to $t = 350$ au and it coincides with the minimum of the

Table 1. CC-CV2$^-$ and TDSE (between parenthesis) normalized partial wave populations of the first ATI peak: $E = 0.199$ ($\omega = 0.35$), $E = 0.249$ ($\omega = 0.375$), $E = 0.288$ ($\omega = 0.4$).

l	$\omega = 0.35$	$\omega = 0.375$	$\omega = 0.4$
0	0.014 (0.018)	0.130 (0.131)	0.139 (0.588)
1	0.000 (0.000)	0.000 (0.000)	0.000 (0.000)
2	0.985 (0.982)	0.870 (0.869)	0.861 (0.412)
3	0.000 (0.000)	0.000 (0.000)	0.000 (0.000)
4	0.000 (0.000)	0.000 (0.000)	0.000 (0.000)

Table 2. CC-CV2$^-$ and TDSE (between parenthesis) normalized partial wave populations of the second ATI peak: $E = 0.548$ ($\omega = 0.35$), $E = 0.624$ ($\omega = 0.375$), $E = 0.691$ ($\omega = 0.4$).

l	$\omega = 0.35$	$\omega = 0.375$	$\omega = 0.4$
0	0.000 (0.000)	0.000 (0.000)	0.000 (0.000)
1	0.304 (0.183)	0.206 (0.544)	0.226 (0.943)
2	0.000 (0.000)	0.000 (0.000)	0.000 (0.000)
3	0.696 (0.816)	0.794 (0.455)	0.774 (0.057)
4	0.000 (0.000)	0.000 (0.000)	0.000 (0.000)

1s population taking into account that about this time the population has almost completely been transferred to the resonant 2p state (see figure 3). The insets show a comparison of close-coupling and TDSE populations at discrete times t_i. Again, we note that the simple close-coupling procedure explains the full TDSE calculations. It should be remarked that only a small set of TDSE results is considered and, therefore, the oscillating structure shown by the close-coupling calculation cannot be accounted for.

For a more detailed test of the CC-CV2$^-$ theory, we analyse the angular momentum of ejected electrons. In table 1 (2) the partial wave populations for energies corresponding to the first (second) ionization peak for three laser frequencies are shown. Only CC-CV2$^-$ and TDSE (between parenthesis) results are shown. Table 1 shows that the first ATI peak is dominated by d- followed by s-electrons for the frequencies analysed. On the other hand, the second ionization peak consists of p- and f-electrons. The dominance of even orbital quantum numbers at the first ATI peak (table 1) and odd orbital quantum numbers at the second ATI peak (table 2) is a direct consequence of the quantum selection rules which are strictly true for infinitely long pulses. The overall explanation is clear. Near resonance, the process around the first (second) ATI peak is dominated by a two-(three-)step process. In the first step, the resonant p-state is populated, a further photon absorption leading to either s- or d-states (table 1) gives rise to the first ATI peak and finally a two-photon absorption for the second ATI peak leads to p- and f-states (table 2). For the first ATI peak, the CC-CV2$^-$ theory describes this general behaviour fairly well and accounts accurately for the partial wave populations for frequencies below the resonance but quantitatively fails for frequencies above. For the resonance frequency, the partial wave populations of the first peak are reproduced by the CC-CV2$^-$ very well. However, there are differences between the CC-CV2$^-$ and the exact TDSE calculations for the second ATI peak. The CC-CV2$^-$ partial wave populations turned out to be rather more insensitive to frequency than what exact TDSE results show.

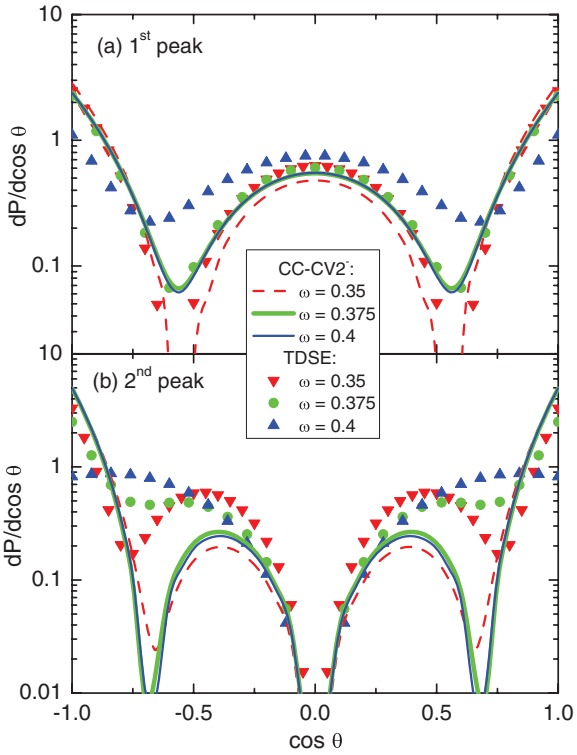

Figure 5. Angular distribution $\mathrm{d}P/\mathrm{d}\cos(\theta)$ as a function of the cosine of the ejection angle θ for electrons emitted with kinetic energy (a) $E = 0.199$ (red), $E = 0.249$ (green) and $E = 0.288$ (blue), corresponding to the first ATI peak for laser frequencies $\omega = 0.35$, $\omega = 0.375$ and $\omega = 0.4$, respectively; and (b) $E = 0.548$ (red), $E = 0.624$ (green) and $E = 0.691$ (blue), corresponding to the second ATI peak, for laser frequencies $\omega = 0.35$, $\omega = 0.375$ and $\omega = 0.4$, respectively. The remaining laser parameters are the same as in figure 1. Lines: CC-CV2$^-$; symbols: TDSE.

In figure 5 the CC-CV2$^-$ normalized angular distributions of ejected electrons are compared with the TDSE results. For the first ATI peak in figure 5(a), the CC-CV2$^-$ results are in very good agreement with TDSE for frequencies below and at resonance. In addition to the forward and backward maxima, a clear maximum is displayed at the centre (electron angles perpendicular to the polarization direction) giving rise to an angular distribution with two minima, i.e. $\theta \simeq 0.31\pi$, and 0.69π proper of d-states. For the frequency higher than resonance, the present theory departs from TDSE displaying a behaviour rather independent of the frequency. The discrepancy comes from the failure of the CC-CV2$^-$ to account properly for the $l = 0$ component as observed in table 1. So the d-component regarding the first ATI peak is overestimated. The angular distribution of ejected electrons with kinetic energy corresponding to the second ATI peak becomes more complex in the full TDSE calculations and some qualitative differences are readily appreciated (see figure 5(b)). However, both TDSE and CC-CV2$^-$ results do exhibit a zero in the direction perpendicular to the laser polarization a characteristic feature of odd orbital quantum numbers. Whereas TDSE angular distributions show some

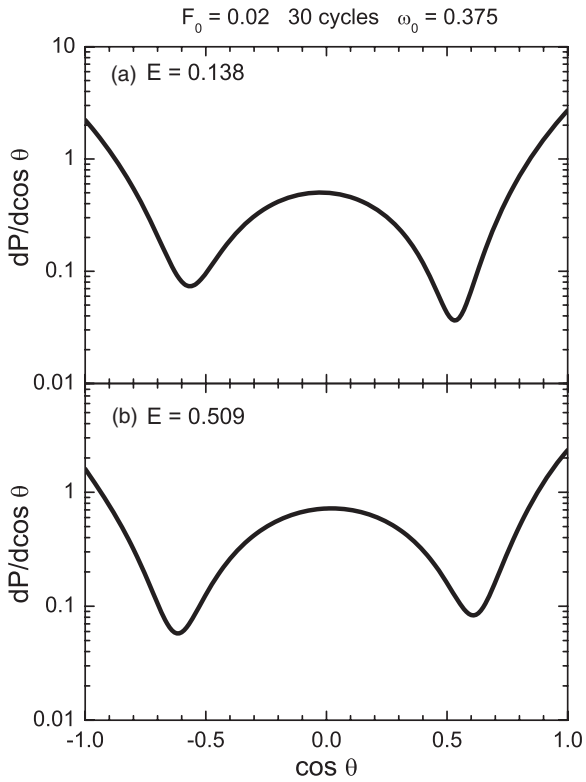

Figure 6. TDSE angular distribution $\mathrm{d}P/\mathrm{d}\cos(\theta)$ as a function of the cosine of the ejection angle θ for electrons emitted with kinetic energy (a) $E = 0.138$ and (b) $E = 0.509$ for laser frequency $\omega_0 = 0.375$. The remaining laser parameters are the same as in figure 1.

Table 3. TDSE normalized partial wave populations at energies on the left ($E = 0.138$) and the right ($E = 0.509$) of the first ATI peak at resonant frequency ($\omega_0 = 0.375$).

l	$E = 0.138$	$E = 0.509$
0	0.116	0.173
1	0.005	0.046
2	0.878	0.774
3	0.000	0.006
4	0.000	0.000

variations for different frequencies, the CC-CV2$^-$ results are again rather independent of frequency.

We now focus on the background, where no resonant behaviour is expected, i.e. energies are quite different from the already defined ϵ_{Mn}. In table 3, the TDSE results with the resonant frequency $\omega_0 = 0.375$ are shown. The whole process involves two photons: the first one populates the resonant 2p state, and the second one increases the electron kinetic energy to either the first valley ($E \simeq 0.14$, first column) or the second valley ($E \simeq 0.51$, second column) in the photoelectron angular distribution (table 3). Thus, no major differences are observed between the two cases where the d-electrons are dominant followed by s-electrons. This pattern is reflected in the angular distribution shown in figure 6, displaying a characteristic distribution of an s and d mixing, almost symmetric with respect to the direction perpendicular to the field polarization. The small asymmetry arises from the $l = 1$ population (table 3).

4. Conclusions

By comparing CV2$^-$ with TDSE, we have been able to establish the importance of the pathways through the bound states when the laser frequency has been tuned accordingly. CV2$^-$ underestimates both the ionization spectrum and the total ionization probabilities and has proved to have a quantitative predicting value only when the laser frequency is larger than the ionization potential. This is a strong indication that intermediate states should be included in the theory, something particularly true when the resonance condition to any bound state is satisfied. In fact, we have shown that for moderate laser intensities it was necessary to employ more accurate transition amplitudes. The MCV2$^-$, whose transition amplitudes are considered simply within the first Born approximation, accounts for the 1s–2p resonance but fails to give accurate total ionization probabilities and energy distributions. This is why a more elaborate theory is needed. The CC-CV2$^-$ considers the time-dependent amplitudes obtained from solving the close-coupling equations for the TDSE using a few bound sates including at least the initial and the resonant states. A great improvement in the total ionization probability and photoelectron spectrum with respect to the MCV2$^-$ has been achieved with the CC-CV2$^-$. In order to probe the CC-CV2$^-$, the partial wave populations and angular distributions based on the theory and numerical results obtained by solving the TDSE are compared. The CC-CV2$^-$ reproduces the general behaviour of TDSE results fairly well, mainly for frequencies below and at resonance ($\omega_0 = 0.375$) but the quantitative agreement is poor for frequencies above the resonance.

Acknowledgments

This work has been supported by CONICET under PIP 112-200801-01269 and 112-200901-00552 and University of Buenos Aires under Projects X843, X147 and 200-200902-00169.

References

[1] Agostini P, Fabre F, Mainfray G, Petite G and Rahman N 1979 *Phys. Rev. Lett.* **42** 1127
[2] Federov M V 1997 *Atomic and Free Electrons in a Strong Light Field* (Singapore: World Scientific)
[3] Delone N B and Krainov V P 2000 *Multiphoton Processes in Atoms* (Berlin: Springer)
[4] Hansch P, Walker M A and Van Woerkom L D 1997 *Phys. Rev.* A **55** R2535
[5] Hertlein M P, Bucksbaum P H and Muller H G 1997 *J. Phys. B: At. Mol. Opt. Phys.* **30** L197
[6] Paulus G G, Grasbon F, Walther H, Kopold R and Becker W 2001 *Phys. Rev.* A **64** 021401
[7] Nandor M J, Walker M A, Van Woerkom L D and Muller H G 1999 *Phys. Rev.* A **60** R1771
[8] Cormier E, Garzella D, Breger P, Agostini P, Chériaux G and Leblanc C 2000 *J. Phys. B: At. Mol. Opt. Phys.* **34** L9

[9] Grasbon F, Paulus G G, Walther H, Villoresi P, Sansone G, Stagira S, Nisoli M and De Silvestri S 2003 *Phys. Rev. Lett.* **91** 173003
[10] Freeman R R, Bucksbaum P H, Milchberg H, Darack S, Schumacher D and Geusic M E 1987 *Phys. Rev. Lett.* **59** 1092
[11] Kopold R, Becker W, Kleber M and Paulus G G 2002 *J. Phys. B: At. Mol. Opt. Phys.* **35** 217
[12] Rudenko A, Zrost K, Schröter C D, de Jesus V L B, Feuerstein B, Moshammer R and Ullrich J 2004 *J. Phys. B: At. Mol. Opt. Phys.* **37** L407
[13] Arbó D G, Yoshida S, Persson E, Dimitriou K I and Burgdörfer J 2006 *Phys. Rev. Lett.* **96** 143003
Arbó D G, Dimitriou K I, Persson E and Burgdörfer J 2008 *Phys. Rev.* A **78** 013406
[14] Alnaser A S, Maharjan C M, Wang P and Litvinyuk I V 2006 *J. Phys. B: At. Mol. Opt. Phys.* **39** L323
[15] Abu-samha M and Madsen L B 2008 *J. Phys. B: At. Mol. Opt. Phys.* **41** 151001
[16] Rodríguez V D 2006 *Nucl. Instrum. Methods Phys. Res.* B **247** 105
[17] Autler S H and Townes C H 1955 *Phys. Rev.* **100** 703
[18] Duchateau G, Cormier E and Gayet R 2002 *Phys. Rev.* A **66** 023412
[19] Macri P A, Miraglia J E and Gravielle M S 2003 *J. Opt. Soc. Am.* B **20** 1801
[20] Girju M G, Hristov K, Kidun O and Bauer D 2007 *J. Phys. B: At. Mol. Opt. Phys.* **40** 4165
[21] Demkov Yu N 1963 *Variational Principles in the Theory of Collisions* (Oxford: Pergamon)
[22] Rodríguez V D, Cormier E and Gayet R 2004 *Phys. Rev.* A **69** 053402